

Toward spatio-temporal models to support national-scale forest carbon monitoring and reporting

Elliot S. Shannon^{1,2}, Andrew O. Finley^{1,2},
Grant M. Domke³, Paul B. May⁴, Hans-Erik Andersen⁵,
George C. Gaines III⁶, Sudipto Banerjee⁷

¹Dept. of Forestry, Michigan State University, East Lansing, MI, USA.

²Dept. of Statistics and Probability, Michigan State University, East Lansing, MI, USA.

³USDA Forest Service, Northern Research Station, St. Paul, MN, USA.

⁴Dept. of Mathematics, South Dakota SMT, Rapid City, SD, USA.

⁵USDA Forest Service, Pacific Northwest Research Station, Seattle, WA, USA.

⁶USDA Forest Service, Rocky Mountain Research Station, Missoula, MT, USA.

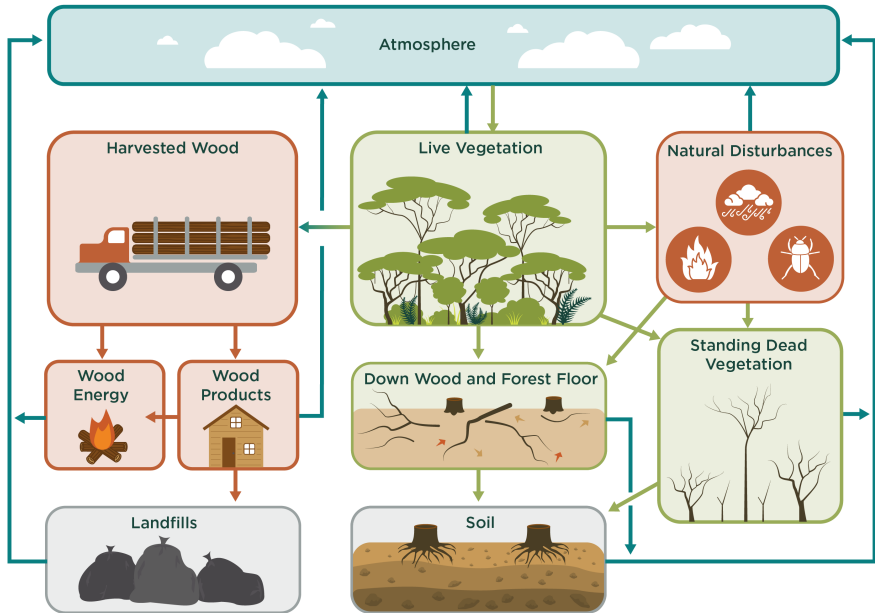
⁷Dept. of Biostatistics, University of California, Los Angeles, Los Angeles, CA, USA.

February 7, 2025



Figure 1: Shannon et al. (2024)

Carbon Cycle



Overview and motivation

- United Nations Framework Convention on Climate Change (UNFCCC) requires annual greenhouse gas (GHG) emission estimates (with uncertainty quantification) from five sectors:

- ▶ Energy
- ▶ Industry
- ▶ Agriculture
- ▶ **Forestry**
- ▶ Waste



- Forest carbon estimates are based on National Forest Inventory (NFI) data and estimators. The US NFI is conducted by the USDA Forest Service Forest Inventory and Analysis (FIA) program.

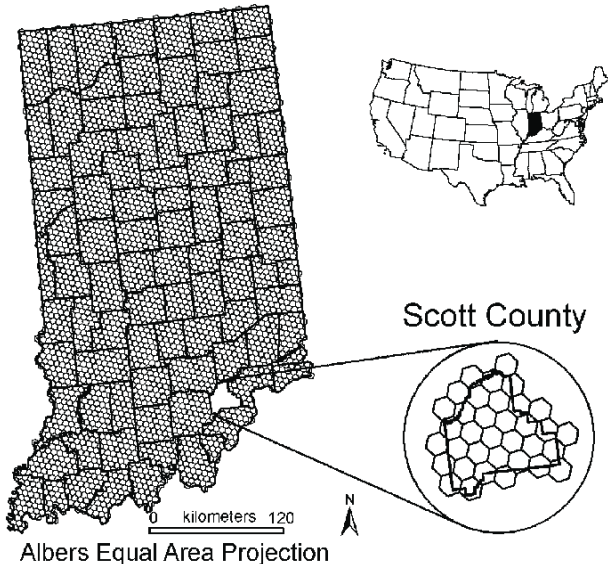


Figure 3: Mcroberts et al. (2005)

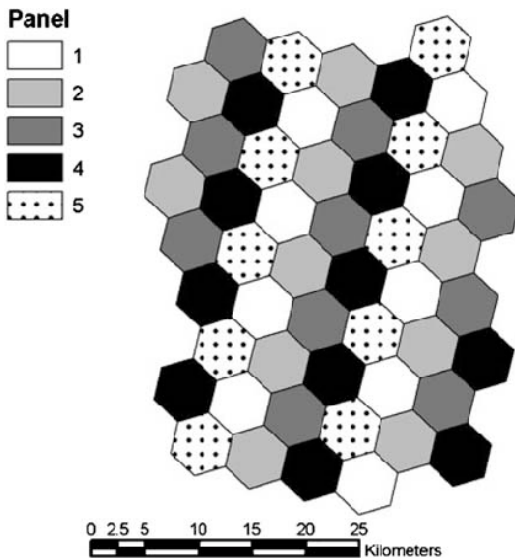


Figure 4: Perry et al. (2009)

Overview and motivation

- NFI programs traditionally use design-based inference based on probability sampling and associated estimators to deliver forest parameter estimates—typically estimates for status parameters.
- Depending on the desired level of estimate precision, such approaches often require costly measurements over a network of inventory plots.
- Increased demand for estimates within smaller spatial, temporal, and biophysical extents than design-based inference can reasonably deliver using current methods.
- Developing model-based small area estimation (SAE) methods using NFI data is an active area of research, with considerable progress made in the last several years (Hou et al., 2021; Coulston et al., 2021; Schroeder et al., 2014; Lister et al., 2020; May et al., 2023; Finley et al., 2024).

Inferential goals

Provide CONUS county estimates of live aboveground forest carbon density for 2008-2021 using FIA county-level direct (i.e., design-based) estimates.

Desired qualities of the estimator:

- ① leverage spatially and temporally proximate information from FIA county estimates and ancillary data to improve estimate accuracy and precision,
- ② provide robust and flexible uncertainty quantification,
- ③ facilitate statistically defensible exploration of carbon status, trend, and change,
- ④ accommodate missing direct estimates,
- ⑤ scale to allow for a large number of areal units and time steps.

Inferential route

SAE methods can generally be classified into **unit-level** and **area-level** models.

- **Unit-level** models are constructed at the level of population units, where a population unit is defined as the minimal unit that can be sampled from a population. Unit-level models typically relate outcome variable measurements on sampled population units to auxiliary data that is available for all population units. Prediction for a small area is achieved by aggregating unit-level predictions within the given areal extent see, e.g., Finley et al. (2024).
- **Area-level** models are constructed across areal units where relationships are built between area-specific outcome direct estimates (e.g., generated using design-based estimators) and auxiliary data (Rao and Molina, 2015). Hence, area-level models effectively “adjust” direct estimates given auxiliary information.

Data

Data for CONUS 2008-2021:

- ① 100k+ plot-level aboveground live tree carbon measurements expressed on as Mg/ha,
- ② a complete set of annual county-level predictor variables.

Let $y_{i,j,t}$ represent the observed carbon density for FIA plot i in county j and year t , where $i = 1, \dots, n_{j,t}$, $j = 1, \dots, J$, and $t = 1, \dots, T$, with $n_{j,t}$ being the number of FIA plots measured in county j and year t .

We consider $J = 3108$ counties and $T = 14$ years.

A set of p annual county-level predictors $x_{k,j,t}$ for $k = 1, \dots, p$.

Data

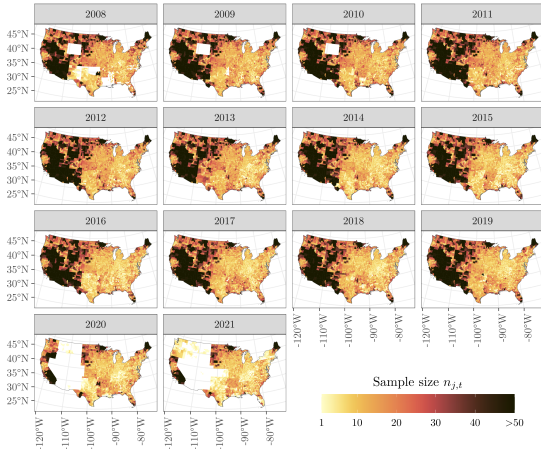


Figure 5: Number of observed FIA plots within each county and year. Transparent counties have zero observed FIA plots ($n_{j,t}$).

Data

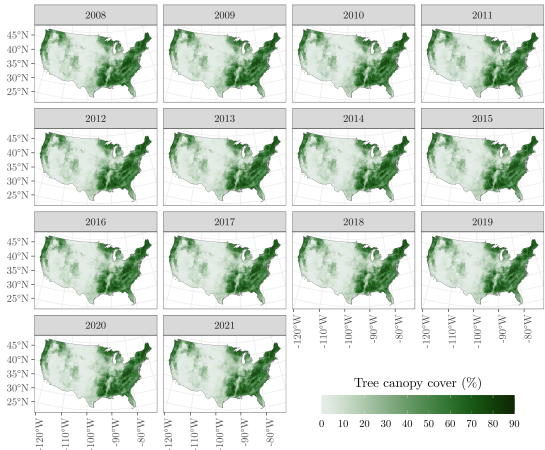


Figure 6: Annual National Land Cover Database percent tree canopy cover (TCC) averaged within each county.

Direct estimates

We assume FIA data are SRS within county and year. When $n_{j,t} \geq 1$ the direct estimate for the population mean is

$$\hat{\mu}_{j,t} = \frac{1}{n_{j,t}} \sum_{i=1}^{n_{j,t}} y_{i,j,t}. \quad (1)$$

and when $n_{j,t} \geq 2$ the estimate variance for (1) is

$$\hat{\sigma}_{j,t}^2 = \frac{1}{n_{j,t}(n_{j,t} - 1)} \sum_{i=1}^{n_{j,t}} (y_{i,j,t} - \hat{\mu}_{j,t})^2. \quad (2)$$

Direct Estimates

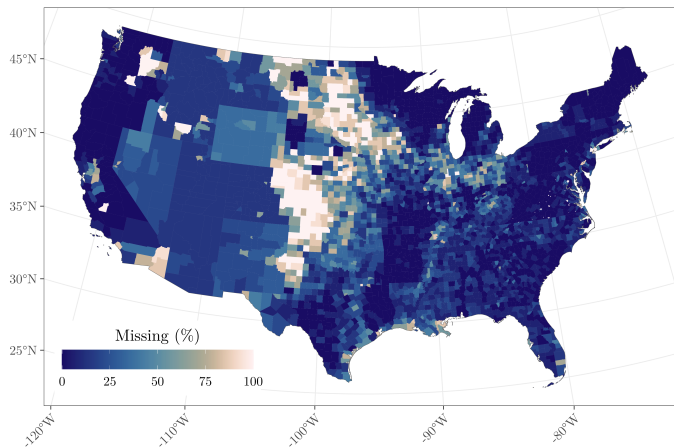


Figure 7: Percent of missing direct estimates across all years.

Proposed SAE model

The model we propose is an extension to the traditional Fay-Herriot model. For county j at time t the model is

$$\hat{\mu}_{j,t} = \mu_{j,t} + \delta_{j,t}, \quad (3)$$

$$\mu_{j,t} = \beta_0 + \eta_{0,j,t} + \sum_{k=1}^p x_{k,j,t} \beta_k + \sum_{k=1}^q \tilde{x}_{k,j,t} \eta_{k,j,t} + \epsilon_{j,t}, \quad (4)$$

where $\delta_{j,t}$ and $\epsilon_{j,t}$ are mutually exclusive error terms with $\delta_{j,t} \stackrel{ind}{\sim} N(0, \sigma_{j,t}^2)$ and $\epsilon_{j,t} \stackrel{iid}{\sim} N(0, \sigma_\epsilon^2)$.

Here, $\delta_{j,t}$'s variance $\sigma_{j,t}^2 \sim IG\left(\frac{n_{j,t}}{2}, \frac{(n_{j,t}-1)\hat{\sigma}_{j,t}^2}{2}\right)$. Modeling $\sigma_{j,t}^2$ in this way provides a more coherent hierarchical model and allows us to obtain potential information from the observed sample size $n_{j,t}$.

Spatial random effects

Consider specifications for the $(q + 1)$ spatial and temporal random effects, i.e., intercept and q for those predictor variables with space-and/or time-varying relationships with the outcome.

We define a $J \times 1$ vector of spatial random effects as

$$\boldsymbol{\eta}^s \sim MVN \left(\mathbf{0}, \sigma_{\eta^s}^2 \mathbf{R}(\rho_{\eta^s}) \right), \quad (5)$$

where $\sigma_{\eta^s}^2$ is the scalar variance, ρ_{η^s} is the correlation parameter, and $\mathbf{R}(\rho_{\eta^s}) = (\mathbf{D} - \rho_{\eta^s} \mathbf{W})^{-1}$ is the $J \times J$ correlation matrix reflecting a conditional autoregressive (CAR) spatial structure, see, e.g., Banerjee et al. (2004).

Spatial random effects

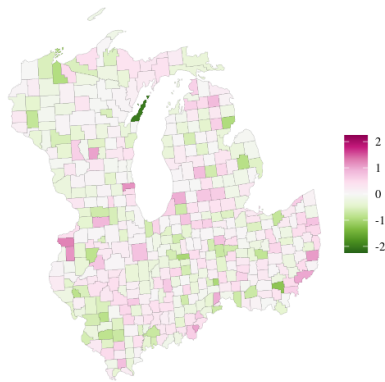


Figure 8: $\sigma_{\eta^s}^2 = 1$ and $\rho_{\eta^s} = 0.2$.

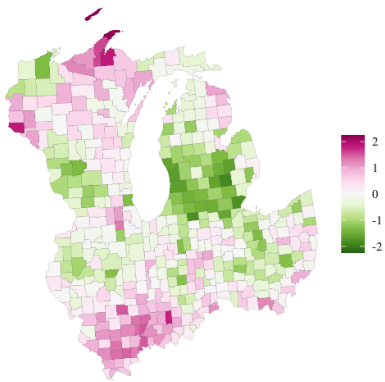


Figure 9: $\sigma_{\eta^s}^2 = 1$ and $\rho_{\eta^s} = 0.99$.

Temporal random effects

When collecting all $N = JT$ space and time observations (stacked by county), we define a $N \times 1$ vector of temporal random effects as

$$\boldsymbol{\eta}^t \sim MVN \left(\mathbf{0}, \sigma_{\eta^t}^2 \mathbf{I} \otimes \mathbf{A}(\alpha_{\eta^t}) \right), \quad (6)$$

where $\sigma_{\eta^t}^2$ is a scalar variance, \mathbf{I} is a $J \times J$ identity matrix, \otimes is the Kronecker product operator, and $\mathbf{A}(\alpha_{\eta^t})$ is a $T \times T$ first order autoregressive correlation matrix with temporal correlation parameter α_{η^t} .

This specification allows for county-specific temporal effects, but does not accommodate spatial association between counties.

Temporal random effects

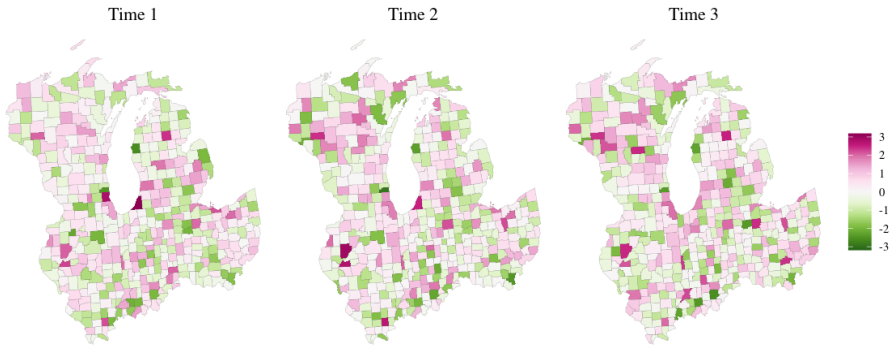


Figure 10: $\sigma_{\eta^t}^2 = 1$ and $\alpha_{\eta^t} = 0.8$.

Spatio-temporal random effects

Finally, we define a $N \times 1$ vector of spatial-temporal random effects as

$$\boldsymbol{\eta}^{st} \sim MVN \left(\mathbf{0}, \sigma_{\eta^{st}}^2 \mathbf{R}(\rho_{\eta^{st}}) \otimes \mathbf{A}(\alpha_{\eta^{st}}) \right), \quad (7)$$

where $\sigma_{\eta^{st}}^2$ is a scalar variance, and all other terms were defined previously.

This specification allows for a county-specific spatial effect to evolve over time.

Spatio-temporal random effects

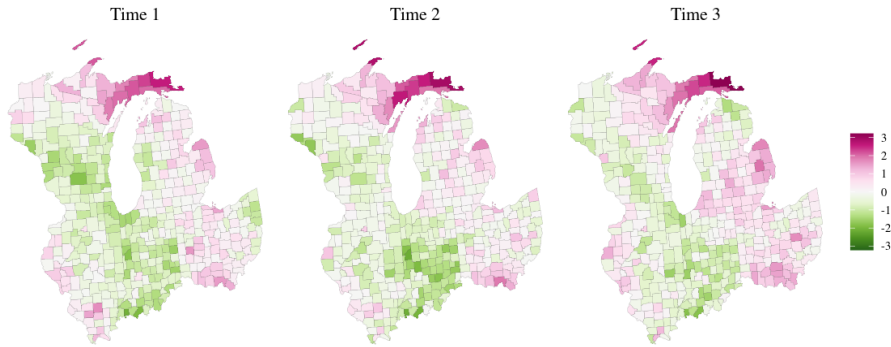


Figure 11: $\sigma_{\eta^{st}}^2 = 1$, $\rho_{\eta^{st}} = 0.99$, and $\alpha_{\eta^{st}} = 0.8$.

Candidate models

In subsequent analyses, we consider the following candidate models for $\mu_{j,t}$.

Each model uses a single predictor variable $x_{TCC,j,t}$, which is percent tree canopy cover (TCC) per county and year (Housman et al., 2023).

$$\text{Full model: } \mu_{j,t} = \beta_0 + \eta_{0,j,t}^{st} + x_{TCC,j,t} \beta_{TCC} + \tilde{x}_{TCC,j,t} \eta_{TCC,j}^s + \epsilon_{j,t}$$

$$\text{Submodel 1: } \mu_{j,t} = \beta_0 + \eta_{0,j,t}^{st} + x_{TCC,j,t} \beta_{TCC} + \epsilon_{j,t}$$

$$\text{Submodel 2: } \mu_{j,t} = \beta_0 + \eta_{0,j,t}^t + x_{TCC,j,t} \beta_{TCC} + \epsilon_{j,t}$$

Full Model

To complete the Bayesian model specification, we assign prior distributions to the model parameters. For the full model, the joint posterior distribution for all parameters is proportional to

$$\begin{aligned} & \prod_{j=1}^J \prod_{t=1}^T N\left(\hat{\mu}_{j,t} \mid \mu_{j,t}, \sigma_{j,t}^2\right) \times \prod_{j=1}^J \prod_{t=1}^T N\left(\mu_{j,t} \mid \beta_0 + \eta_{0,j,t}^{st} + \sum_{k=1}^p x_{k,j,t} \beta_k + \sum_{k=1}^q \tilde{x}_{k,j,t} \eta_{k,j}^s, \sigma_{\epsilon}^2\right) \times \\ & \prod_{k=0}^p N\left(\beta_k \mid \mu_{\beta}, \sigma_{\beta}^2\right) \times \prod_{j=1}^J \prod_{t=1}^T IG\left(\sigma_{j,t}^2 \mid \frac{n_{j,t}}{2}, \frac{(n_{j,t}-1) \hat{\sigma}_{j,t}^2}{2}\right) \times IG\left(\sigma_{\epsilon}^2 \mid a_{\epsilon}, b_{\epsilon}\right) \times \\ & MVN\left(\boldsymbol{\eta}_0^{st} \mid \mathbf{0}, \sigma_{\eta^{st}}^2 \mathbf{R}(\rho_{\eta^{st}}) \otimes \mathbf{A}(\alpha_{\eta^{st}})\right) \times \\ & IG\left(\sigma_{\eta_0^{st}}^2 \mid a_{\eta_0^{st}}, b_{\eta_0^{st}}\right) \times U\left(\rho_{\eta_0^{st}} \mid a_{\rho}, b_{\rho}\right) \times U\left(\alpha_{\eta_0^{st}} \mid a_{\alpha}, b_{\alpha}\right) \times \\ & \prod_{k=1}^q MVN\left(\boldsymbol{\eta}_k^s \mid \mathbf{0}, \sigma_{\eta_k^s}^2 \mathbf{R}(\rho_{\eta_k^s})\right) \times \prod_{k=1}^q IG\left(\sigma_{\eta_k^s}^2 \mid a_{\eta^s}, b_{\eta^s}\right) \times \prod_{k=1}^q U\left(\rho_{\eta_k^s} \mid a_{\rho}, b_{\rho}\right). \end{aligned} \tag{8}$$

Simulation Study

- A single population is generated using fixed and known values for parameters, then estimates for parameters are computed from each of a large number of independent samples, i.e., R replicates, taken from the population.
- Estimates are then compared with population parameters using a set of measures that assess the estimators' bias, accuracy, and precision.

Simulation Study

- To mimic qualities of the observed annual county-level data, we simulated a population comprising 7,809,952 point-referenced population units laid out in a 1-by-1 (km) regular grid over the CONUS land area.
- Specifically, the outcome $y_t(\ell)$ at generic population unit location ℓ and time t is given by

$$y_t(\ell) = \zeta_0 + u_t(\ell) + \zeta_1 v_{TCC,t}(\ell) + \epsilon_t(\ell), \quad \epsilon_t(\ell) \stackrel{iid}{\sim} N(0, \sigma_y^2),$$

$$u_t(\ell) = u_{t-1}(\ell) + w_t(\ell), \quad u_0(\ell) = 0,$$

$$w_t(\ell) \stackrel{ind}{\sim} GP(0, C(\cdot, \gamma)), \quad t = 1, 2, \dots, T,$$

- $C(\cdot, \gamma) = \sigma_w^2 \exp(-\gamma ||\ell - \ell'||)$

Simulation Study

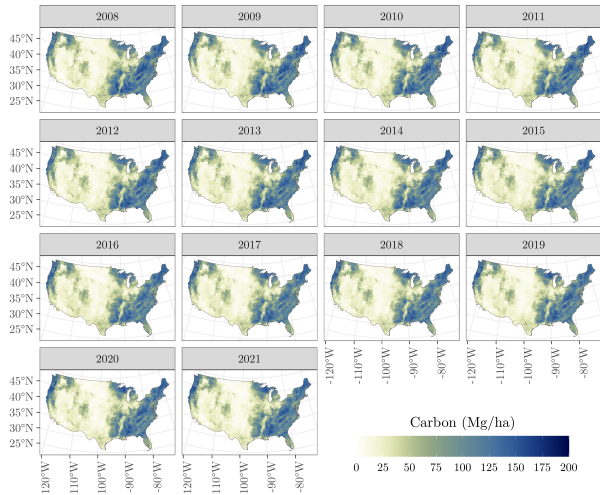


Figure 12: Simulated population forest carbon density $\mu_{\text{true},t,j}$ (Mg/ha).

Simulation Study

Given $\mu_{true,j,t}$ and R estimates from each estimator,

$$\text{Bias}_{j,t,I} = \frac{\sum_{r=1}^R (\mu_{j,t,I,r} - \mu_{true,j,t})}{R}, \quad (9)$$

$$\text{RMSE}_{j,t,I} = \sqrt{\frac{\sum_{r=1}^R (\mu_{j,t,I,r} - \mu_{true,j,t})^2}{R}}. \quad (10)$$

$$\text{Coverage}_{j,t,I} = \frac{\sum_{r=1}^R I(\mu_{j,t,I,r}^L \leq \mu_{true,j,t} \leq \mu_{j,t,I,r}^U)}{R}, \quad (11)$$

$$\text{Width}_{j,t,I} = \frac{\sum_{r=1}^R (\mu_{j,t,I,r}^U - \mu_{j,t,I,r}^L)}{R}. \quad (12)$$

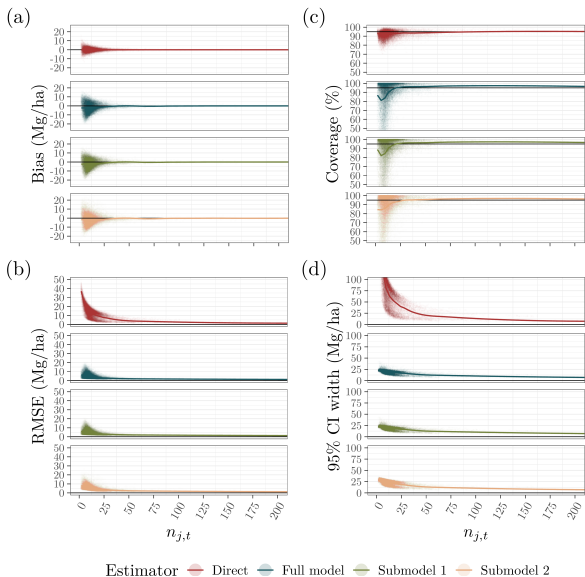


Figure 13: Point values represent averages over R replicates for a county and year. A loess line is added to indicate trends across sample size ($n_{j,t}$).

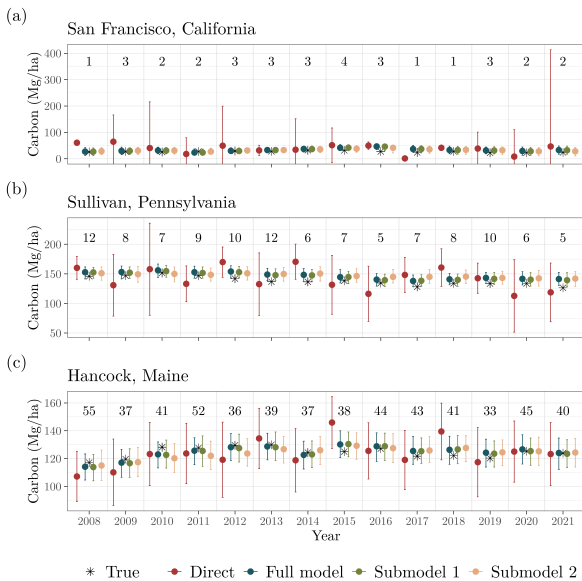


Figure 14: Simulated $\mu_{true,j,t}$ values and estimates based on sample data from the first replicate.

Table 1: Parameter estimates for candidate models fit to FIA data. Estimates are posterior medians with 95% credible intervals given in parentheses. Estimates for WAIC and associated statistics are given in the last several rows. The last row holds the estimated $\widehat{\text{elpd}}_{\text{WAIC}}$ difference with the “best” fitting Submodel 1 and associated standard error $\widehat{\tau}_{\text{diff}}$ in parentheses.

Parameter	Candidate models		
	Submodel 2	Submodel 1	Full model
β_0	18.15 (17.92, 18.38)	18.39 (18.00, 18.79)	13.83 (12.48, 15.13)
β_{TCC}	15.27 (15.04, 15.53)	18.43 (18.16, 18.83)	16.08 (15.05, 17.18)
$\alpha_{\eta_0^t}$	0.9982 (0.9979, 0.9985)	-	-
$\sigma_{\eta_0^t}^2$	75.73 (71.61, 80.29)	-	-
$\rho_{\eta_0^{st}}$	-	0.9995 (0.9990, 0.9998)	0.9996 (0.9993, 0.9998)
$\alpha_{\eta_0^{st}}$	-	0.9966 (0.9961, 0.9972)	0.9969 (0.9963, 0.9975)
$\sigma_{\eta_0^{st}}^2$	-	140.37 (130.31, 150.30)	86.81 (79.14, 94.11)
$\rho_{\eta_{TCC}^s}$	-	-	0.9999 (0.9995, 1.0000)
$\sigma_{\eta_{TCC}^s}^2$	-	-	34.71 (28.55, 41.29)
σ_ϵ^2	0.70 (0.61, 0.79)	0.59 (0.54, 0.66)	0.56 (0.51, 0.63)
$\widehat{\text{elpd}}_{\text{WAIC}}$	-113123.6	-112481.2	-112496.2
$\widehat{\rho}_{\text{WAIC}}$	7078.1	6622.7	6461.9
WAIC	226247.3	224962.4	224992.4
$\widehat{\text{elpd}}_{\text{diff}}$	-642.5 (51.9)	0 (0)	-15.0 (22.2)

FIA analysis

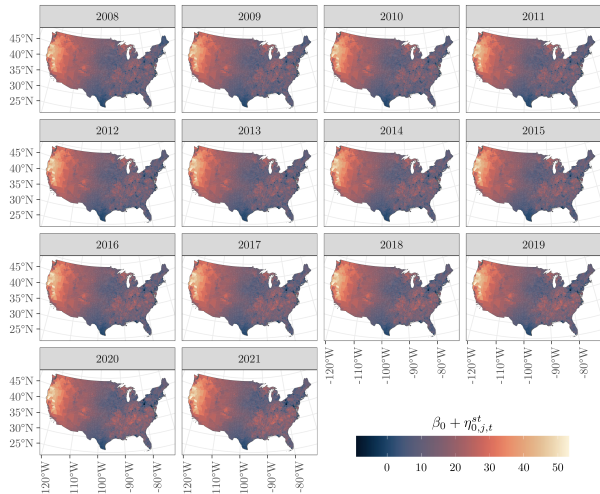


Figure 15: Full model's $\beta_0 + \eta_{0,j,t}^{st}$.

FIA analysis

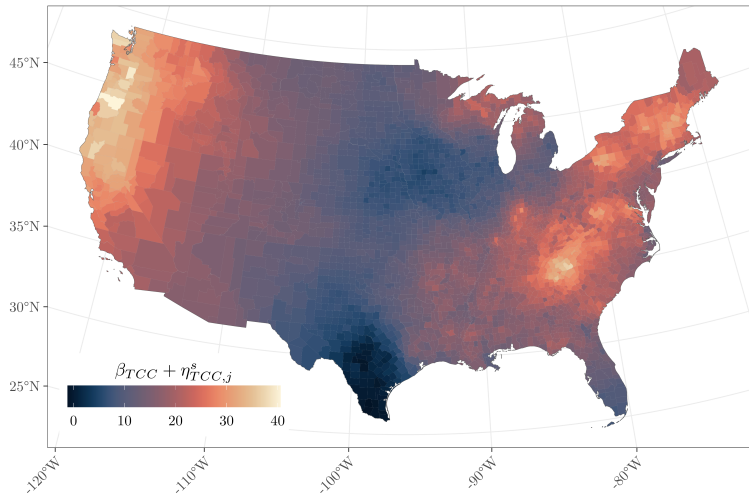


Figure 16: Full model's $\beta_{TCC} + \eta_{TCC,j}^s$ (i.e., strong evidence of a nonstationary relationship between TCC and carbon density). TCC was scaled and centered.

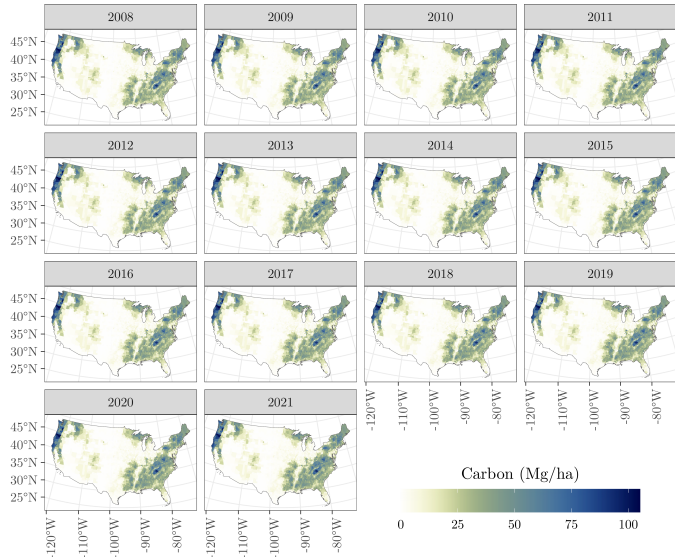


Figure 17: Full model's $\mu_{j,t}$ posterior mean.

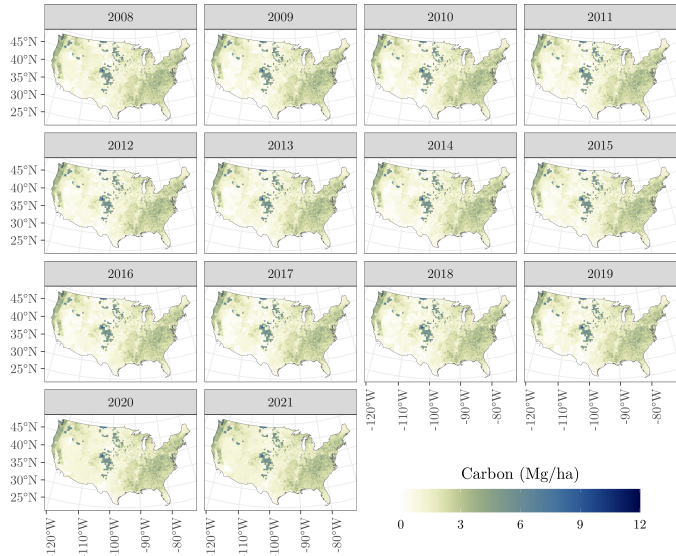


Figure 18: Full model's $\mu_{j,t}$ posterior standard deviation.

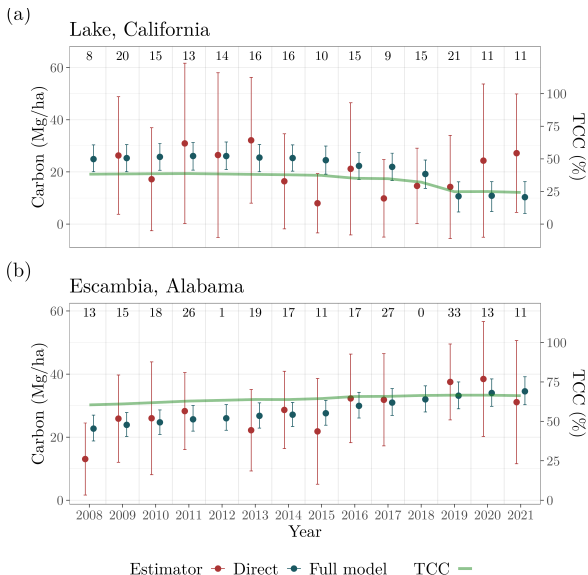


Figure 19: Direct and Full model estimates of $\hat{\mu}_{j,t}$ and $\mu_{j,t}$, respectively, for a few county j 's and $t = 1, \dots, T$, along with associated 95% confidence and credible intervals.

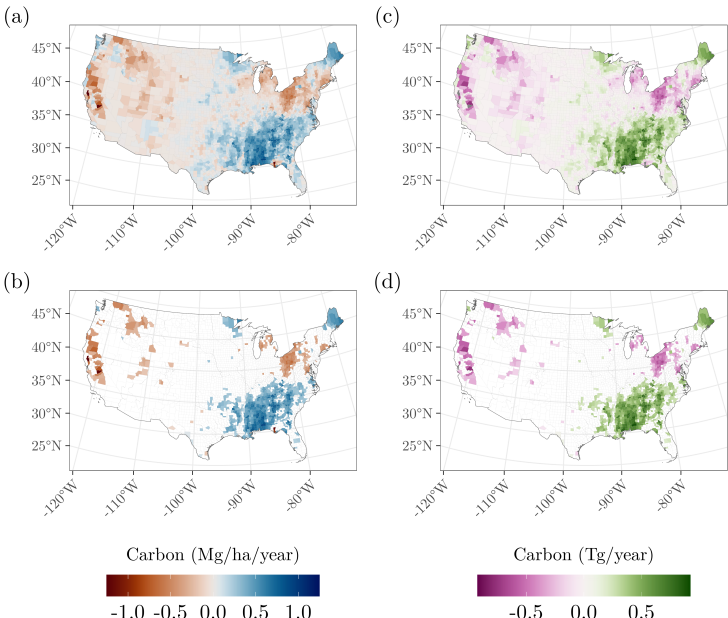


Figure 20: Posterior mean of linear trend in carbon Mg/ha/year over 2008-2021.

Table 2: Ten largest decreasing and increasing estimates of total carbon trends (Tg/year) from 2008 to 2021 across the CONUS. Estimates are posterior medians with 95% credible interval values given in parentheses.

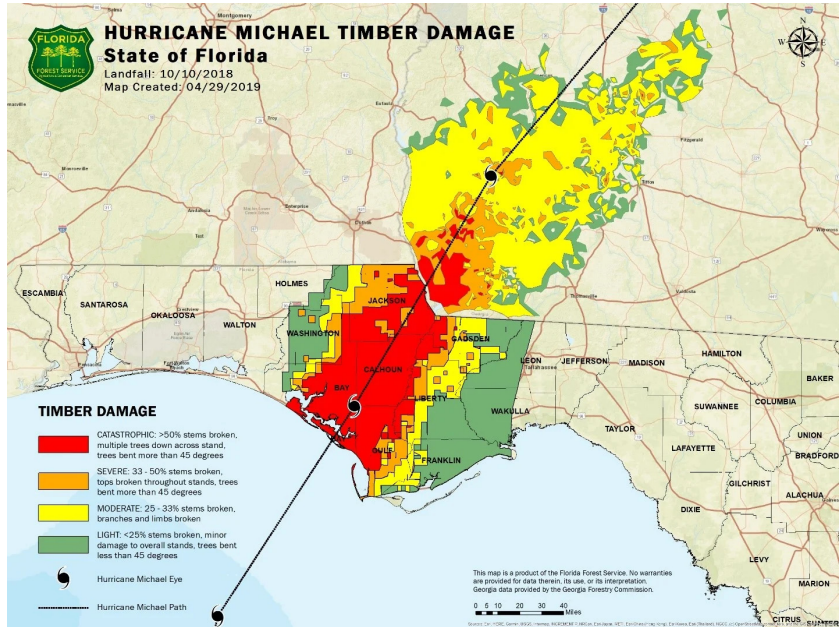
Decreasing			Increasing		
State	County	Carbon	State	County	Carbon
Idaho	Idaho	-0.92 (-1.41, -0.45)	Maine	Aroostook	0.71 (0.35, 1.05)
California	Siskiyou	-0.92 (-1.33, -0.48)	Minnesota	St. Louis	0.64 (0.34, 0.96)
California	Shasta	-0.7 (-0.98, -0.44)	Maine	Piscataquis	0.57 (0.31, 0.83)
Washington	Okanogan	-0.69 (-1.00, -0.36)	Maine	Penobscot	0.49 (0.29, 0.68)
Oregon	Douglas	-0.47 (-0.87, -0.11)	Maine	Washington	0.46 (0.26, 0.64)
California	Mariposa	-0.45 (-0.60, -0.29)	Maine	Somerset	0.44 (0.22, 0.66)
California	Tuolumne	-0.45 (-0.61, -0.28)	Alabama	Baldwin	0.29 (0.19, 0.40)
California	Lake	-0.43 (-0.56, -0.30)	Maine	Hancock	0.27 (0.14, 0.40)
California	Trinity	-0.43 (-0.67, -0.20)	Minnesota	Cook	0.25 (0.08, 0.43)
California	Fresno	-0.42 (-0.73, -0.11)	Minnesota	Itasca	0.24 (0.07, 0.42)



HURRICANE MICHAEL TIMBER DAMAGE

State of Florida

Landfall: 10/10/2018
Map Created: 04/29/2019

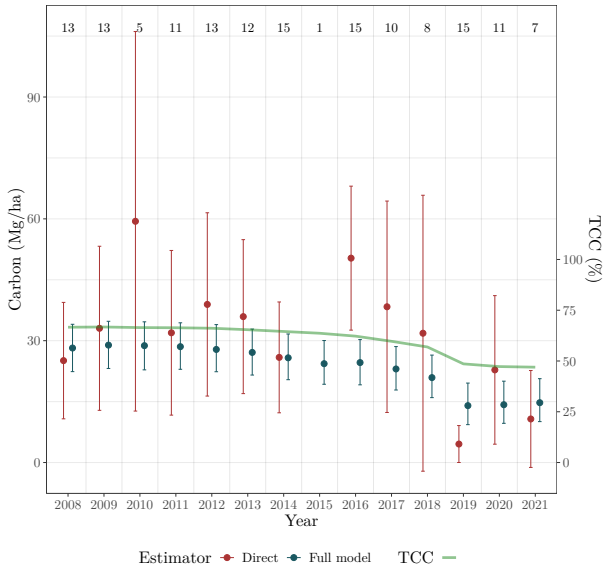


This map is a product of the Florida Forest Service. No warranties are provided for data therein, its use, or its interpretation. Georgia data provided by the Georgia Forestry Commission.

0 5 10 20 30 40 Miles

FIA analysis

Calhoun, Florida



FIA analysis



Figure 21: Timber damage from Hurricane Michael. Photo courtesy of Jarek Nowak, Ph.D., Florida Forest Service.

FIA analysis

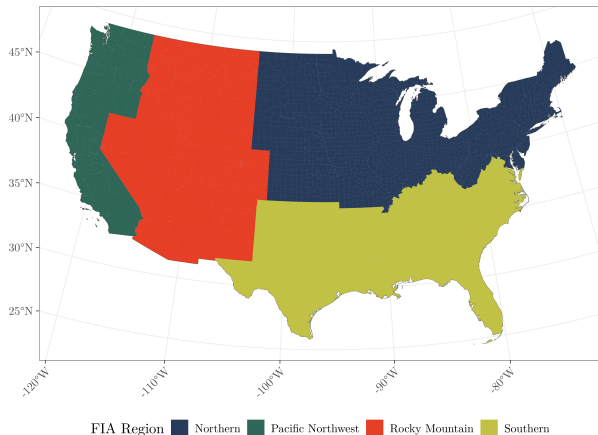


Figure 22: FIA regions used to compute county aggregate total estimates given in Figure 23.

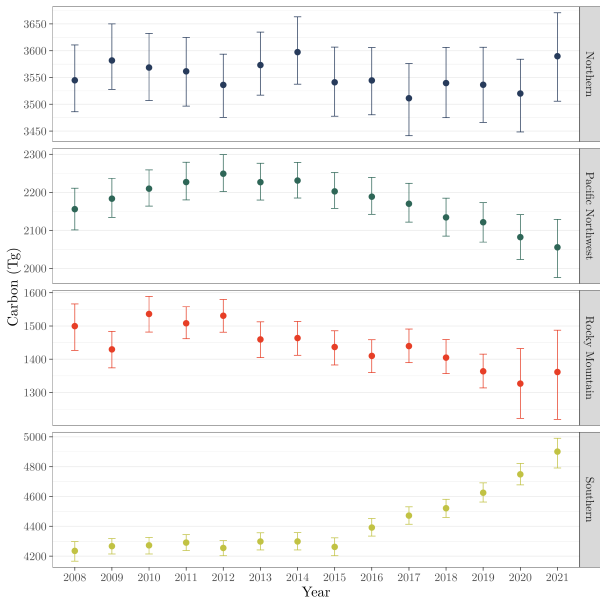


Figure 23: Annual carbon within FIA regions shown in Figure 22. Point and bars are the Posterior median and 95% credible interval.

FIA analysis

Table 3: Left column, model estimated carbon trend by FIA region from 2008 to 2021. Right column, model estimated total carbon change by FIA region between 2008 and 2021. Estimates are medians with 95% credible interval values given in parentheses.

FIA Region	Trend (Tg/year)	Change (Tg)
Northern	-1.94 (-6.74, 3.42)	43.03 (-43.05, 137.98)
Pacific Northwest	-9.55 (-14.71, -5.34)	-101.01 (-186.91, -23.12)
Rocky Mountain	-12.86 (-19.46, -6.13)	-137.03 (-285.29, -1.29)
Southern	44.32 (36.83, 50.55)	660.45 (534.73, 781.08)

Summary and next steps

- Promising initial modeling results in terms of uncertainty quantification and spatial and temporal trend detection.
- Continuing with simulation study to assess model's inferential pros and cons.
- Considering extensions for carbon change attribution.
- Extending this or other spatio-temporal models to accommodate multiple carbon pools.



Thank you

- Banerjee, S., Carlin, B. and Gelfand, A. (2004), *Hierarchical Modeling and Analysis of Spatial Data*, Vol. 101.
- Coulston, J. W., Green, P. C., Radtke, P. J., Prisley, S. P., Brooks, E. B., Thomas, V. A., Wynne, R. H. and Burkhart, H. E. (2021), 'Enhancing the precision of broad-scale forestland removals estimates with small area estimation techniques', *Forestry: An International Journal of Forest Research* **94**(3), 427–441.
- Finley, A. O., Andersen, H.-E., Babcock, C., Cook, B. D., Morton, D. C. and Banerjee, S. (2024), 'Models to support forest inventory and small area estimation using sparsely sampled lidar: A case study involving g-light lidar in tanana, alaska', *Journal of Agricultural, Biological and Environmental Statistics* .
URL: <https://doi.org/10.1007/s13253-024-00611-3>
- Hou, Z., Domke, G. M., Russell, M. B., Coulston, J. W., Nelson, M. D., Xu, Q. and McRoberts, R. E. (2021), 'Updating annual state-and county-level forest inventory estimates with data assimilation and FIA data', *Forest Ecology and Management* **483**, 118777.
- Housman, I., Schleeweis, K., Heyer, J., Ruefenacht, B., Bender, S., Megown, K., Goetz, W. and Bogle, S. (2023), 'National land cover database tree canopy cover methods v2021.4', GTAC-10268-RPT1. Salt Lake City, UT: U.S. Department of Agriculture, Forest Service, Geospatial Technology and Applications Center.
- Lister, A. J., Andersen, H., Frescino, T., Gatziolis, D., Healey, S., Heath, L. S., Liknes, G. C., McRoberts, R. E., Moisen, G. G., Nelson, M. et al. (2020), 'Use of Remote Sensing Data to Improve the Efficiency of National Forest Inventories: A Case Study from the United States National Forest Inventory', *Forests* **11**(12), 1364.
- May, P., McConville, K. S., Moisen, G. G., Bruening, J. and Dubayah, R. (2023), 'A spatially varying model for small area estimates of biomass density across the contiguous united states', *Remote Sensing of Environment* **286**, 113420.
URL: <https://www.sciencedirect.com/science/article/pii/S0034425722005260>
- Mcroberts, R., Wendt, D. and Liknes, G. (2005), 'Stratified estimation of forest inventory variables using spatially summarized stratifications', *Silva Fennica* **39**.
- Perry, C., Woodall, C., Liknes, G. and Schoeneberger, M. (2009), 'Filling the gap: Improving estimates of working tree resources in agricultural landscapes', *Agroforestry Systems* **75**, 91–101.
- Rao, J. N. and Molina, I. (2015), *Small area estimation*, John Wiley & Sons.
- Schroeder, T. A., Healey, S. P., Moisen, G. G., Frescino, T. S., Cohen, W. B., Huang, C., Kennedy, R. E. and Yang, Z. (2014), 'Improving estimates of forest disturbance by combining observations from Landsat time series with US Forest Service Forest Inventory and Analysis data', *Remote Sensing of Environment* **154**, 61–73.
- Shannon, E. S., Finley, A. O., Domke, G. M., May, P. B., Andersen, H.-E., Gaines III, G. C. and Banerjee, S. (2024), 'Toward spatio-temporal models to support national-scale forest carbon monitoring and reporting', *Environmental Research Letters* **20**(1), 014052.
URL: <https://dx.doi.org/10.1088/1748-9326/ad9e07>